Predictive Energy Management Strategy for Fuel Cell Vehicles Combining Long-Term and Short-Term Forecasts

Sandro Kofler, Zhang Peng Du, Stefan Jakubek, and Christoph Hametner

***Abstract*—Fuel cell electric vehicles are usually hybrid vehicles requiring an energy management strategy (EMS) to determine the power split between the fuel cell system and a battery. The performance of an EMS can be improved by taking into account forecasts of the vehicle velocity. Simple estimates derived from static route information, e.g., speed limits, can already provide a significant performance increase because of being available before departure and for the entire driving mission. However, such long-term predictions can deviate considerably from the actual velocity because of dynamic influences, such as traffic, roadworks, or weather. Here, short-term predictions from vehicular communication systems provide more accurate real-time information and allow the EMS to react better to the actual driving conditions. This article proposes a predictive EMS that efficiently combines the information of long-term and short-term forecasts. Before departure, a dynamic programming algorithm optimizes the energy management based on *a-priori* available route data yielding a distance-based map describing the optimal cost-to-go. While driving, a model predictive controller (MPC) optimizes the energy management online considering the information of the short-term prediction and including the optimal cost-to-go as terminal cost. A computationally efficient linear MPC implementation is proposed, and the significant performance benefit over an MPC that tracks an optimized battery state-of-charge reference is demonstrated in a numerical study.**

***Index Terms*—Cost-to-go, dynamic programming, energy management, fuel cell vehicle, fuel optimal control, model predictive control, velocity prediction.**

I. Introduction

FUEL fuel cell electric vehicles (FCEVs) are commonly designed as hybrid vehicles, i.e., their powertrain includes a battery as an auxiliary power source besides the fuel cell system (FCS). The battery allows for recuperating kinetic energy and avoiding low-efficient operation ranges of the FCS [1]. In this way, the hybrid configuration of the powertrain offers benefits in terms of fuel economy, which, however, strongly rely on the energy management, i.e., the power split between FCS and battery. Besides fuel economy, other aspects are associated with the energy management, such as battery charge control and the lifetimes of the power sources: Extremely charging or discharging the battery provokes degradation and might even cause infeasible operation, particularly in the case of heavy-duty vehicles. Therefore, the battery's state of charge (SoC) should remain within a predefined range during operation. To mitigate the degradation of the FCS, dynamic transients and high peaks in the FCS power demand should be avoided [2], [3]. The globally optimal power split considering the aforementioned criteria could only be realized if the power demand of the entire driving mission would be known *a-priori*, which is noncausal [4]. Here, predictive energy management strategies (EMSs) come into play. With an appropriate vehicle model, the future power demand can be estimated based on the altitude and velocity profiles of the upcoming part of a driving mission. Whereas the altitude can directly be derived from topographical data if the route is planned in advance, the velocity must be predicted.

Vehicle velocity prediction is a challenging task due to numerous stochastic influences such as driver behavior, traffic flow, traffic signals, and environmental influences [5], [6], [7]. The uncertainty grows with the length of the prediction horizon, which is why it is impossible to predict the velocity of a human-driven vehicle for an entire driving mission with a high accuracy. An estimate of the velocity along a planned route can be based on *a-priori* available static route information such as speed limits [8], [9], [10]. Even though such a prediction is not very accurate, it can considerably improve the performance because it is available for the entire driving mission in advance. In contrast, more accurate velocity forecasts can be provided by onboard, short-term prediction methods based on intelligent transportation systems (ITSs). In addition to static route information, these methods are provided with real-time information regarding the actual driving conditions, such as traffic, roadworks, or weather, through vehicle-to-vehicle (V2V) and vehicle-to-infrastructure (V2I) communication [11], [12], [13].

In the literature, two-stage EMS approaches are often found to consider long-term predictions of the entire driving mission. Commonly, a reference trajectory for the battery's state of charge (SoC) is optimized based on the long-term prediction in the first stage. This offline optimization is often performed with dynamic programming (DP) [14], [15], which is a numerical method for dynamic optimization problems. The strengths of DP are the capabilities to deal with nonlinear problems and

Manuscript received 7 March 2023; revised 22 November 2023; accepted 00 Xxx 2023. This work was supported with funds from the Climate and Energy Fund and implemented in line with the "Zero Emission Mobility" program. The authors acknowledge the TU Wien Bibliothek for financial support through its Open Access Funding Program.

S. Kofler, Z. P. Du, and S. Jakubek are with the Institute of Mechanics and Mechatronics, TU Wien, 1060 Vienna, Austria (e-mail: sandro.kofler@tuwien.ac.at; zhang.peng.du@tuwien.ac.at; stefan.jakubek@tuwien.ac.at).

C. Hametner is with the Christian Doppler Laboratory for Innovative Control and Monitoring of Automative Powertrain Systems, TU Wien, 1060 Vienna, Austria (e-mail: christoph.hametner@tuwien.ac.at).

Corresponding author: S. Kofler.

consider constraints on inputs and states. In the second stage, an online strategy determines the power split between the primary power source and the battery while driving such that the SoC reference profile is tracked. To improve the performance and react to the actual driving conditions, online strategies can additionally take into account the more accurate short-term predictions, e.g., based on model predictive control (MPC), an optimal control framework allowing to consider constraints and predictions within a certain prediction horizon [14], [16], [17].

However, using SoC reference trajectories to consider feedforward information has a drawback. Optimized long-term information of the remaining trip is only available along the SoC reference trajectory. If the actual power demand deviates from the underlying long-term forecast, which is likely because the forecast is only based on static route information, the actual SoC is expected to deviate from its reference. Tracking the SoC reference trajectory, i.e., forcing the SoC back to the reference, is a suboptimal behavior [18]. Of course, the reference trajectory could be re-optimized, but this requires additional computational resources.

An effective alternative to consider optimized long-term information is the optimal cost-to-go [19], which can be computed with DP [20], [18], [21]. The optimal cost-to-go describes the minimum amount of fuel needed to reach the intended destination as a function of the position along the trip and the SoC. This means that long-term information is available for the entire SoC range in contrast to an SoC reference trajectory. Again, MPC is a suitable basis for additionally considering short-term predictions to react to the actual driving conditions. Here, the optimal cost-to-go can be included as terminal cost in the objective function [20], [22], [23].

Even though cost-to-go-based MPC methods are available in the literature, they focus on hybrid electric vehicles powered by internal combustion engines but not FCEVs. Moreover, the majority of the cost-to-go-based MPCs are based on nonlinear formulations, which might complicate their real-time onboard implementation [24].

The main contribution of this work is a predictive EMS for FCEVs using DP to compute the optimal cost-to-go based on *a-priori* available static route information before departure and a linear, cost-to-go-based MPC taking into account short-term predictions in order to react to actual driving conditions. The distinctive feature of the proposed EMS is that optimized long-term information is considered in the form of the optimal cost-to-go, which, unlike an SoC reference trajectory, provides information within the entire SoC range. Consequently, optimized information is available even if the actual SoC completely deviates from the originally optimal path. The DP algorithm used to conduct the offline optimization allows to consider state and input constraints and can handle nonlinearities. The computational complexity of the DP, which is often reported to be a limiting factor [21], [23], is kept low because only one state is involved and a rather rough discretization is sufficient for the optimization based on the long-term prediction derived from static route information. The offline DP yields the optimal cost-to-go in the form of a 2-D map depending on the position along the trip and the SoC. Here, a distance-based rather than a time-based description of the cost-to-go is chosen to be independent of the actual velocity, which is initially unknown. The online energy management is conducted with an MPC considering real-time, short-term predictions within the prediction horizon and an approximation of the optimal cost-to-go as terminal cost. In this way, the MPC efficiently combines the short-term prediction with the optimized long-term information and minimizes the amount of fuel for the trip remainder in each instant. The proposed MPC is based on a computationally efficient, linear formulation, which is highly beneficial for the onboard implementation.

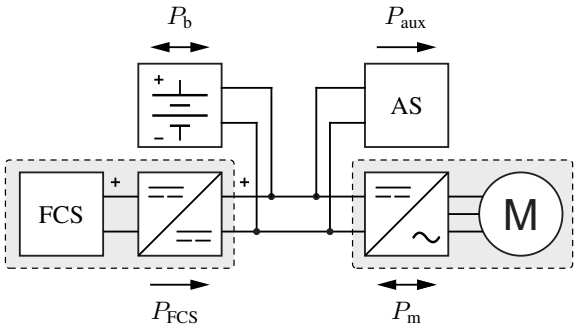

Fig. 1: Hybrid vehicle configuration consisting of FCS, battery, traction motor, and auxiliary systems (AS). The arrows indicate the possible directions of the power flows.

The remainder of this article is structured as follows. First, a control-oriented model of the FCEV is presented in Section II. Then, the proposed EMS is described in Section III, followed by the linear formulation of the MPC in Section IV. In Section V, the proposed MPC is compared to an MPC that tracks an optimized SoC reference trajectory. The comparison is based on the simulation of a real-world driving cycle. A conclusion finalizes this article.

II. System Modeling

Optimizing the energy management requires knowledge of the future vehicle power demand and the powertrain dynamics. A prediction of the power demand is not directly available but can be derived from a forecast of the vehicle velocity considering longitudinal vehicle dynamics. In the following, control-oriented models of the vehicle and the hybrid powertrain dynamics are described.

A. Vehicle Dynamics

The longitudinal model of the vehicle considers the traction, aerodynamic drag, rolling resistance, and gravitational force and is expressed by

$$\delta m \frac{\mathrm{d}v}{\mathrm{d}t} = \frac{P_\mathrm{tr}}{v} - \frac{\rho A_\mathrm{f} c_\mathrm{d}}{2} v^2 - c_\mathrm{r} m g \cos\theta - m g \sin\theta \quad (1)$$

where v denotes the vehicle velocity, t the time, m the vehicle mass, δ the correction coefficient of rotating mass, ρ the air density, A_f the vehicle frontal area, c_d the drag coefficient, c_r the rolling resistance coefficient, g the gravitational acceleration, and θ the inclination angle of the road. The traction

power P_{tr} is provided by an electric motor. The input power of the motor

$$P_{\mathrm{m}} = P_{\mathrm{tr}}\, \eta_{\mathrm{m}}^{-\operatorname{sgn} P_{\mathrm{tr}}} \tag{2}$$

includes power losses in the inverter and the motor approximated by the efficiency η_{m}. The overall electric power demand P_{el} of the vehicle is the sum of the motor input power and the power consumption of the auxiliary systems P_{aux}:

$$P_{\mathrm{el}} = P_{\mathrm{m}} + P_{\mathrm{aux}}. \tag{3}$$

With that, a prediction of the electric power demand can be derived from predictions of the vehicle velocity and the inclination angle of the road.

B. Hybrid Powertrain

The vehicle is equipped with a hybrid powertrain with two power sources, the FCS and a battery (see Fig. 1). Whereas the FCS can only provide power, the battery can also store energy coming from the FCS or the electric motor during regenerative braking. The sum of the FCS power P_{FCS} and the battery power P_{b} satisfies the overall electric load:

$$P_{\mathrm{el}} = P_{\mathrm{FCS}} + P_{\mathrm{b}}. \tag{4}$$

The hybrid configuration of the powertrain implies one degree of freedom, i.e., the power split between the FCS and the battery. The EMS determines the FCS power, which is assumed to be provided within reasonable time. The residual of the power demand is provided by the battery, subject to the corresponding constraints.

The FCS is considered in the form of a simplified, quasistatic model determined by measurements, where the fuel consumption rate $\dot{m}_{\mathrm{H_2}}$ of the FCS is a monotonically increasing function of the FCS power. The FCS model implicitly considers the losses in the converter and the power demand of the corresponding auxiliaries, such as the compressor.

The battery is modeled in the form of an equivalent circuit model with three parameters: the open-circuit voltage V_{OC}, the internal battery resistance R_{int}, and the nominal battery capacity Q_0 [25]. The dynamics of the battery SoC ξ is described by a nonlinear function depending on the battery power:

$$\frac{\mathrm{d}\xi}{\mathrm{d}t} = f(P_{\mathrm{b}}) = -\frac{V_{\mathrm{OC}} - \sqrt{V_{\mathrm{OC}}^2 - 4P_{\mathrm{b}}R_{\mathrm{int}}}}{2Q_0R_{\mathrm{int}}}. \tag{5}$$

With this control-oriented description, the dynamic model of the powertrain has only one state, which is the battery SoC.

III. Predictive Energy Management

The proposed predictive EMS comprises two stages. Before departure, the energy management of the hybrid powertrain is optimized based on a long-term prediction of the power demand, which is available for the entire driving mission. This *offline optimization* is conducted by DP and yields a 2-D map describing the optimal cost-to-go, i.e., the minimum amount of fuel required to reach the intended destination, as a function of the position along the trip and the SoC.

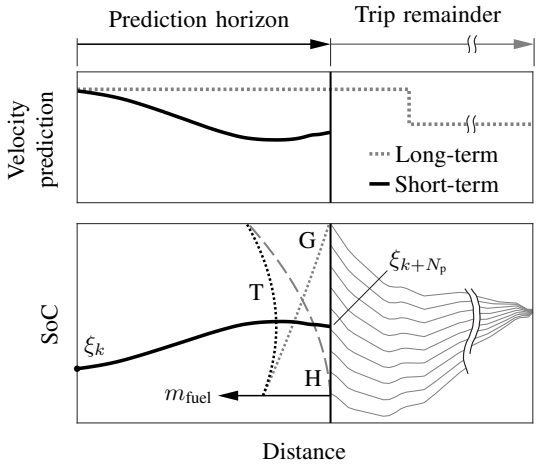

Fig. 2: The MPC optimizes the power split such that the total fuel amount (T), which is the sum of the fuel consumed within the prediction horizon (H) and the optimal cost-to-go (G), is minimized. The optimal cost-to-go represents the fuel amount of optimal paths for the trip remainder.

While driving, the *online MPC* successively optimizes the power split considering a more accurate short-term prediction and the optimal cost-to-go at the end of the prediction horizon. Here, the cost-to-go provides optimized long-term information for the entire SoC range. As illustrated in Fig. 2, the cost-to-go decreases with an increasing SoC at the end of the prediction horizon since more energy is available from the battery for the remaining trip. However, a higher SoC at the end of the prediction horizon implies a higher fuel consumption within the horizon because the battery needs to be charged. The optimal power split minimizes the sum of the fuel consumed within the prediction horizon and the cost-to-go.

In the following, the two EMS stages and the corresponding predictions are described in detail.

A. Offline Optimization With Dynamic Programming

The offline optimization of the energy management requires a long-term prediction of the power demand. Planning the route before departure gives access to static route information such as the elevation profile and speed limits. Based on the speed limits, an estimate of the vehicle velocity can be derived considering simplified vehicle dynamics during transients and maximum cornering speeds. With the known elevation profile and the estimated velocity profile, an estimate of the vehicle power demand for the entire driving mission can be derived based on the vehicle model (1) - (3).

The optimization aims at minimizing the fuel consumption for the planned trip under the consideration of the battery

dynamics and constraints

$$\min J = \int_{t_0}^{t_1} \dot{m}_{\mathrm{H_2}}(P_{\mathrm{FCS}}(t))\mathrm{d}t \tag{6a}$$
$$\text{s.t.} \quad P_{\mathrm{FCS}}(t) \in \mathcal{U} \tag{6b}$$
$$P_{\mathrm{b}}(t) \in \mathcal{B} \tag{6c}$$
$$\xi(t) \in \mathcal{X} \tag{6d}$$
$$\xi(t_0) = \xi_0 \tag{6e}$$
$$\xi(t_1) \in \mathcal{X}_1 \tag{6f}$$

where the sets $\mathcal{U}$, $\mathcal{B}$, $\mathcal{X}$, and $\mathcal{X}_1$ cover the feasible values according to the specified constraints on the FCS power, the battery power, the SoC, and the terminal SoC, respectively, and ξ_0 denotes the initial SoC. The set $\mathcal{X}_1$ is commonly specified by a minimum boundary for the final SoC. Based on Bellman's principle of optimality, the discrete counterpart of the dynamic optimization problem can be solved by a recursive backward algorithm known as dynamic programming [26]. For this purpose, the battery model (5) is discretized assuming a zero-order hold for the power demand and the FCS power giving

$$\xi_{l+1} = \xi_l - \frac{V_{\mathrm{OC}} - \sqrt{V_{\mathrm{OC}}^2 - 4(P_{\mathrm{el},l} - P_{\mathrm{FCS},l})R_{\mathrm{int}}}}{2Q_0 R_{\mathrm{int}}}\Delta t_l \tag{7}$$

where $\Delta t_l = t_{l+1} - t_l$. The problem is solved in the distance domain meaning that the trip is divided into $N-1$ distance segments. Consequently, Δt_l varies depending on the velocity and the length of the segment, and sections where the vehicle velocity is zero are ignored. The mean power demand of the l-th segment is derived from the prediction with

$$P_{\mathrm{el},l} = \frac{\int_{t_l}^{t_{l+1}} P_{\mathrm{el}}\,\mathrm{d}t}{\Delta t_l}. \tag{8}$$

The DP algorithm optimizes a sequence of subproblems starting at the position $N-1$ and successively stepping backwards until the beginning of the trip:

$$J_l^*(\xi_l) = \min_{P_{\mathrm{FCS},l}} \left[\dot{m}_{\mathrm{H_2}}(P_{\mathrm{FCS},l})\Delta t_l + J_{l+1}^*(\xi_{l+1})\right] \tag{9a}$$
$$\text{s.t.} \; P_{\mathrm{FCS},l} \in \mathcal{U}^{\mathrm{q}} \tag{9b}$$
$$P_{\mathrm{b},l} \in \mathcal{B} \tag{9c}$$
$$\xi_{l+1} \in \mathcal{X}_{l+1} \tag{9d}$$
$$\forall \xi_l \in \mathcal{X}^{\mathrm{q}}$$
$$\forall l \in \{1, \ldots, N-1\}.$$

The finite sets $\mathcal{U}^{\mathrm{q}}$ and $\mathcal{X}^{\mathrm{q}}$ result from the quantization of $\mathcal{U}$ and $\mathcal{X}$, respectively. The set $\mathcal{X}_{l+1} \subseteq \mathcal{X}$ covers the feasible states at the position $l+1$ subject to the constraints. The resulting optimal cost-to-go function $J_l^*(\xi_l)$ describes the minimum amount of fuel needed to reach the intended destination from the position l as a function of the SoC. The optimal cost-to-go is stored as a discrete map for each position of the distance grid. Moreover, the boundaries $\xi_l^{\min}$ and $\xi_l^{\max}$ of $\mathcal{X}_l$ are stored for all positions.

The computational complexity of the DP algorithm grows linearly with the number of segments and, thus, linearly with the length of the long-term prediction if an equidistant segmentation is chosen. However, the complexity can be kept low because a rather rough segmentation is sufficient for the offline optimization due to the limited accuracy of the long-term prediction. To save further computational time, the step size can also be determined adaptively depending on the power demand signal [27].

B. Online Model Predictive Control

Since the long-term prediction is only based on static route information, a deviation from the actual power demand because of dynamic influences, such as traffic, roadworks, or weather, is inevitable. To improve the performance and better react to the actual driving conditions, the online MPC additionally considers short-term predictions. Such predictions can be provided by forecasting systems considering V2V and V2I communication [11] and are expected to be more accurate than the long-term prediction because, in addition to static route data, they include real-time information.

The objective function of the MPC consists of two terms, the fuel consumption within the prediction horizon and a terminal cost

$$J_k = \sum_{j=k}^{k+N_{\mathrm{p}}-1} \dot{m}_{\mathrm{H_2}}(P_{\mathrm{FCS},j})T_{\mathrm{s}} + J_{k+N_{\mathrm{p}}}^*(\xi_{k+N_{\mathrm{p}}}(\boldsymbol{P}_{\mathrm{FCS},k})) \tag{10}$$

where T_{s} denotes the constant sampling time and $\boldsymbol{P}_{\mathrm{FCS},k} = [P_{\mathrm{FCS},k}, \ldots, P_{\mathrm{FCS},k+N_{\mathrm{p}}-1}]^{\mathrm{T}}$ denotes the sequence of the FCS power within the prediction horizon of N_{p} samples. The index k denotes quantities at the current instant. Note that the indexing based on k is independent of the indexing based on l used in the DP. The terminal cost represents the cost-to-go at the end of the prediction horizon, which is obtained by distance-based interpolation in the cost-to-go map resulting from the offline optimization. It is a function of the terminal SoC and, therefore, the sequence of control inputs.

The optimal sequence of control inputs at the instant k is determined by minimizing the objective function

$$\boldsymbol{P}_{\mathrm{FCS},k}^* = \arg\min_{\boldsymbol{P}_{\mathrm{FCS},k}} J_k \tag{11a}$$
$$\text{s.t.} \; P_{\mathrm{FCS},k+n} \in \mathcal{U}, \quad \forall n \in \{0, \ldots, N_{\mathrm{p}}-1\} \tag{11b}$$
$$\Delta P_{\mathrm{FCS},k+n} \in \mathcal{R}, \; \forall n \in \{0, \ldots, N_{\mathrm{p}}-1\} \tag{11c}$$
$$P_{\mathrm{b},k+n} \in \mathcal{B}, \quad \forall n \in \{0, \ldots, N_{\mathrm{p}}-1\} \tag{11d}$$
$$\xi_{k+n} \in \mathcal{X}, \quad \forall n \in \{1, \ldots, N_{\mathrm{p}}-1\} \tag{11e}$$
$$\xi_{k+N_{\mathrm{p}}} \in \mathcal{X}_{k+N_{\mathrm{p}}} \tag{11f}$$

with

$$\Delta P_{\mathrm{FCS},k} = P_{\mathrm{FCS},k} - P_{\mathrm{FCS},k-1} \tag{12}$$

whereby the short-term power demand prediction is considered as disturbance. The set $\mathcal{R}$ describes constraints on the increments of the FCS power, which are necessary to avoid requesting infeasible transients from the FCS. The consideration of these constraints is only relevant in the MPC because the offline DP is based on a considerably rougher discretization, where the FCS dynamics are negligible. The boundaries $\xi_{k+N_{\mathrm{p}}}^{\min}$ and $\xi_{k+N_{\mathrm{p}}}^{\max}$ defining the set of feasible states $\mathcal{X}_{k+N_{\mathrm{p}}}$ at the end of the prediction horizon are determined by distance-based linear interpolation. The battery constraints (11d) as well as

the state constraints (11e) and (11f) are implemented as soft constraints to prevent infeasibility. According to the receding horizon principle, only the first step $P^*_{\mathrm{FCS},k}$ is actually applied to the system. In the next sampling instant, the measurements and the short-term prediction are updated, and the procedure is repeated [28].

The two terms of the objective function have counteracting effects on the optimization. The minimization of the fuel consumption within the prediction horizon is favored by a low FCS power. However, a lower FCS power implies a lower SoC at the end of the prediction horizon and, consequently, a higher cost-to-go because less energy is stored in the battery. The optimal power split is a trade-off and minimizes the amount of fuel needed to reach the intended destination based on the available information, which consists of the short-term prediction and the optimized long-term information.

IV. Linear MPC Formulation

The optimal control problem of the online MPC (11) must be solved onboard and in real time. Therefore, reducing the computational complexity for solving the problem is highly beneficial for the implementation. In this section, a computationally efficient linear MPC formulation is derived. First, the powertrain model is linearized. Then, a local quadratic approximation of the cost-to-go is formulated, and a physically motivated objective function taking into account ohmic battery losses is derived. The formulation allows to constrain increments of the FCS power to prevent the FCS from infeasible power rates.

A. Model Linearization

The battery model (5) is linearized at the operating point $P_{\mathrm{b,op}} = 0\,\mathrm{W}$ yielding

$$\frac{\mathrm{d}\xi}{\mathrm{d}t} = -\frac{P_\mathrm{b}}{Q_0 V_\mathrm{OC}} + R(P_\mathrm{b}) \tag{13}$$

where R denotes the remainder. The linearized model is then discretized with T_s assuming a zero-order hold for the battery power. An incremental formulation of the control input, i.e., the FCS power, is chosen to allow constraining the control moves. Therefore, the state vector includes two states, the SoC and the FCS power: $\boldsymbol{x}_k = [\xi_k\,,\, P_{\mathrm{FCS},k-1}]^\mathrm{T}$. Considering (4), the linear discrete-time state-space model can be written as

$$\boldsymbol{x}_{k+1} = \begin{bmatrix} 1 & -c \\ 0 & 1 \end{bmatrix} \boldsymbol{x}_k + \begin{bmatrix} -c \\ 1 \end{bmatrix} \Delta u_k + \begin{bmatrix} c \\ 0 \end{bmatrix} w_k \tag{14a}$$

$$\boldsymbol{y}_k = \boldsymbol{x}_k \tag{14b}$$

where

$$\Delta u_k = P_{\mathrm{FCS},k} - P_{\mathrm{FCS},k-1}, \quad w_k = P_{\mathrm{el},k}, \quad c = -\frac{T_\mathrm{s}}{Q_0 V_\mathrm{OC}}.$$

Based on the linear model, the future trajectories of the SoC, the FCS power, and the battery power within the prediction horizon can be expressed as

$$\boldsymbol{S}_k = \boldsymbol{F}_\mathrm{S}\,\boldsymbol{x}_k + \boldsymbol{\Phi}_\mathrm{S}\,\Delta\boldsymbol{U}_k + \boldsymbol{\Theta}_\mathrm{S}\boldsymbol{W}_k \tag{15}$$

$$\boldsymbol{P}_{\mathrm{FCS},k} = \boldsymbol{F}_\mathrm{F}\,\boldsymbol{x}_k + \boldsymbol{\Phi}_\mathrm{F}\,\Delta\boldsymbol{U}_k \tag{16}$$

$$\boldsymbol{P}_{\mathrm{b},k} = -\boldsymbol{F}_\mathrm{F}\,\boldsymbol{x}_k - \boldsymbol{\Phi}_\mathrm{F}\,\Delta\boldsymbol{U}_k + \boldsymbol{W}_k \tag{17}$$

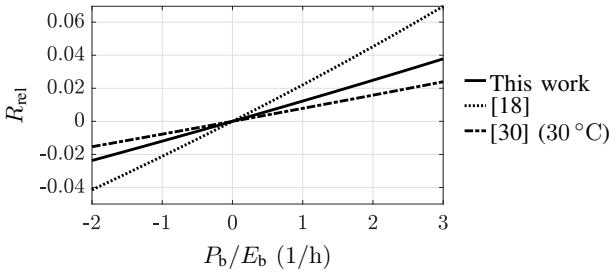

Fig. 3: Relative linearization error of the battery model as a function of the normalized battery power with respect to the nominal battery energy E_b.

and the SoC at the end of the prediction horizon can be expressed as

$$\xi_{k+N_\mathrm{p}} = \bar{\boldsymbol{F}}_\mathrm{S}\boldsymbol{x}_k + \bar{\boldsymbol{\Phi}}_\mathrm{S}\Delta\boldsymbol{U}_k + \bar{\boldsymbol{\Theta}}_\mathrm{S}\boldsymbol{W}_k \tag{18}$$

where

$$\begin{aligned}
\boldsymbol{S}_k &= \begin{bmatrix} \xi_{k+1} & \dots & \xi_{k+N_\mathrm{p}} \end{bmatrix}^\mathrm{T} \\
\boldsymbol{P}_{\mathrm{FCS},k} &= \begin{bmatrix} P_{\mathrm{FCS},k} & \dots & P_{\mathrm{FCS},k+N_\mathrm{p}-1} \end{bmatrix}^\mathrm{T} \\
\boldsymbol{P}_{\mathrm{b},k} &= \begin{bmatrix} P_{\mathrm{b},k} & \dots & P_{\mathrm{b},k+N_\mathrm{p}-1} \end{bmatrix}^\mathrm{T} \\
\Delta\boldsymbol{U}_k &= \begin{bmatrix} \Delta u_k & \dots & \Delta u_{k+N_\mathrm{p}-1} \end{bmatrix}^\mathrm{T} \\
\boldsymbol{W}_k &= \begin{bmatrix} w_k & \dots & w_{k+N_\mathrm{p}-1} \end{bmatrix}^\mathrm{T}.
\end{aligned}$$

The time-invariant matrices $\boldsymbol{F}_\mathrm{S}$, $\boldsymbol{\Phi}_\mathrm{S}$, $\boldsymbol{\Theta}_\mathrm{S}$, etc. are derived from the discrete-time model as described in [29].

The linearization of the battery model implies a linearization error, which is linked to the neglected ohmic losses and, therefore, depends on the battery parameters. The relative linearization error can be computed with

$$R_\mathrm{rel}(P_\mathrm{b}) = \frac{R(P_\mathrm{b})}{f(P_\mathrm{b})} = \frac{V_\mathrm{OC} - \sqrt{V_\mathrm{OC}^2 - 4R_\mathrm{int}P_\mathrm{b}}}{2V_\mathrm{OC}} \tag{19}$$

and is shown for some batteries from the literature in Fig. 3. The approximation is good, in particular, if the battery is operated with low absolute values of the battery power. Moreover, the impact of the linearization on the SoC prediction is limited because the prediction horizon wherein an accurate short-term prediction is feasible is relatively short.

B. Approximation of the Cost-To-Go

The optimal cost-to-go resulting from the offline optimization is available as a discrete map $J^*_l(\xi_l)$ at each position of the distance grid and can be approximated for any position by distance-based linear interpolation. The upper plots in Fig. 4 show typical cost-to-go profiles at two different positions of a driving cycle. The cost-to-go generally decreases with an increasing SoC because more energy is stored in the battery. Under certain conditions, however, the cost-to-go remains constant if a certain threshold ξ_l^th is exceeded. This behavior is illustrated in the plots of position 2, which is almost at the end of the cycle, and can be explained as follows: Suppose that the minimum final SoC specified by $\mathcal{X}_1$ can be reached from the l-th position running the FCS only with the minimum feasible power according to $\mathcal{U}$ if $\xi_l = \xi_l^\mathrm{th}$. Then, the minimum

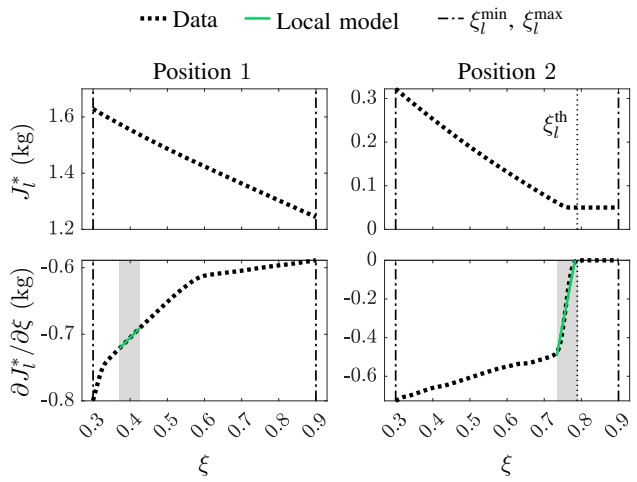

Fig. 4: The optimal cost-to-go resulting from the offline optimization and the partial derivative of the cost-to-go with respect to the SoC at two different position of a driving cycle. The shaded areas in the lower plots indicate exemplary ranges where local linear models are fitted to. Note the differently scaled ordinates.

final SoC is exceeded if $\xi_l > \xi_l^{\text{th}}$ likewise operating the FCS with the minimum feasible power. The amount of fuel to reach the destination, i.e., the cost-to-go, is the same in either case because the fuel consumption rate is only a function of the FCS power. Consequently, the cost-to-go profile remains constant for all $\xi_l \geq \xi_l^{\text{th}}$.

The absolute value of the cost-to-go is irrelevant for the online optimization by the MPC; relevant is the partial derivative of the cost-to-go with respect to the SoC, which can be derived by numerical differentiation. Therefore, the approximation of the cost-to-go is based on a model of the derivative of the cost-to-go. Describing the derivative of the cost-to-go by a uniform function of the SoC is not possible because of the sharp changes in its slope, as the lower plots of Fig. 4 indicate. More details regarding this behavior of the derivative of the cost-to-go are given in Section V-C. Consequently, the derivative of the cost-to-go at the end of the prediction horizon is modeled with a local linear model

$$\left.\frac{\partial \hat{J}^*_{k+N_\text{p}}}{\partial \xi}\right|_{\xi_k} = \beta_0 + \beta_1 \xi_{k+N_\text{p}} \tag{20}$$

where the two parameters β_0 and β_1 are estimated by the least-squares method within a predefined range around ξ_k (note that ξ_{k+N_p} is unknown). The range the local linear model is fitted to lies within $[\xi_l^{\min}; \xi_l^{\text{th}}]$ if the threshold is relevant, otherwise within $[\xi_l^{\min}; \xi_l^{\max}]$.

The cost-to-go at the end of the prediction horizon can then be approximated with a truncated Taylor series, where ξ_k is chosen as operating point

$$J^*_{k+N_\text{p}} = J^*_{k+N_\text{p}}\Big|_{\xi_k} + \left.\frac{\partial \hat{J}^*_{k+N_\text{p}}}{\partial \xi}\right|_{\xi_k} \left(\xi_{k+N_\text{p}} - \xi_k\right). \tag{21}$$

The first term in (21) is irrelevant for the optimization as it does not depend on the decision variable and, therefore, omitted. Inserting (20) gives the local quadratic approximation of the optimal cost-to-go

$$\hat{J}^*_{k+N_\text{p}} = \left(\beta_0 - \beta_1 \xi_k\right) \xi_{k+N_\text{p}} + \beta_1 \xi^2_{k+N_\text{p}} \tag{22}$$

where another constant term has been omitted likewise.

C. Quadratic Objective Function

The objective function for the linear MPC considers the fuel consumption within the prediction horizon and the cost-go-to at the end of the prediction horizon as in (10). The components of the objective function are elaborated in the following.

1) Online cost: The quasistatic FCS model is approximated with a second-order polynomial model:

$$\hat{\dot{m}}_{\text{H}_2} = \gamma_0 + \gamma_1 \cdot P_\text{FCS} + \gamma_2 \cdot P^2_\text{FCS}. \tag{23}$$

This allows to express the first term of the objective function in (10) with a quadratic formulation based on the future FCS power sequence (16)

$$m_{\text{H}_2,k} = \gamma_0 + \mathbf{q}_1^\text{T} \boldsymbol{P}_{\text{FCS},k} + \boldsymbol{P}^\text{T}_{\text{FCS},k} \mathbf{Q}_2 \boldsymbol{P}_{\text{FCS},k} \tag{24}$$

with

$$\mathbf{q}_1 = \gamma_1 T_\text{s} \begin{bmatrix} 1 & 1 & \dots & 1 \end{bmatrix}^\text{T}, \qquad \mathbf{q}_1 \in \mathbb{R}^{N_\text{p} \times 1} \tag{25}$$

$$\mathbf{Q}_2 = \gamma_2 T_\text{s} \boldsymbol{I}, \qquad \mathbf{Q}_2 \in \mathbb{R}^{N_\text{p} \times N_\text{p}} \tag{26}$$

where $\boldsymbol{I}$ denotes the identity matrix.

The battery model is linearized at $P_{\text{b,op}} = 0\,\text{W}$ in (13), i.e., ohmic battery losses

$$P_\Omega = R_\text{int} I_\text{b}^2 \tag{27}$$

are not considered in the linear model the MPC is based on. Therefore, a physically motivated equivalent fuel consumption representing the ohmic battery losses is included in the objective function, which is based on a quadratic approximation. With $I_\text{b} = -Q_0 \dot{\xi}$ and the nonlinear battery model (5) follows

$$I_\text{b}^2 = \left(\frac{V_\text{OC} - \sqrt{V_\text{OC}^2 - 4 P_\text{b} R_\text{int}}}{2 R_\text{int}} \right)^2. \tag{28}$$

Truncating the Taylor series of (28) at $P_{\text{b,op}} = 0\,\text{W}$ after the quadratic term yields

$$I_\text{b}^2 = \frac{P_\text{b}^2}{V_\text{OC}^2}. \tag{29}$$

An approximation of the equivalent fuel consumption rate can then be written after inserting (29) into (27) and assuming a mean FCS efficiency $\bar{\eta}_\text{FCS}$

$$\dot{m}_\text{eq} = \frac{R_\text{int}}{V_\text{OC}^2 \, \bar{\eta}_\text{FCS} \, H_\text{i}} P_\text{b}^2 \tag{30}$$

where H_i denotes the lower heating value of hydrogen. With that, the equivalent fuel consumption within the prediction horizon can be formulated as

$$m_{\text{eq},k} = \boldsymbol{P}^\text{T}_{\text{b},k} \mathbf{Q}_\Omega \boldsymbol{P}_{\text{b},k} \tag{31}$$

where the weighting matrix $\mathbf{Q}_\Omega$ is determined by

$$\mathbf{Q}_\Omega = \frac{R_\text{int} \, T_\text{s}}{V_\text{OC}^2 \, \bar{\eta}_\text{FCS} \, H_\text{i}} \boldsymbol{I}, \quad \mathbf{Q}_\Omega \in \mathbb{R}^{N_\text{p} \times N_\text{p}}. \tag{32}$$

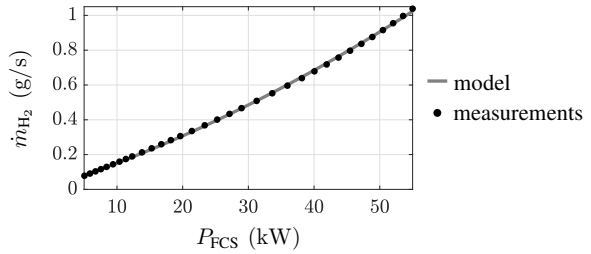

Fig. 5: Fuel consumption rate of the FCS as a function of the FCS power: steady-state measurements vs. polynomial model.

2) Cost-to-go: The cost-to-go is considered in the form of the quadratic approximation in (22).

3) Overall objective function: The overall quadratic objective function is the sum of (22), (24), and (31)

$$\hat{J}_k = m_{\mathrm{H_2},k} + m_{\mathrm{eq},k} + \hat{J}^*_{k+N_\mathrm{p}} \tag{33}$$

and represents the amount of fuel required to go from the current position to the intended destination.

In each instant, the linear MPC solves the optimal control problem specified in (11) whereby J_k is replaced by $\hat{J}_k$, which turns the problem into a quadratic programming problem and reduces the computational complexity. Quadratic programming can be solved in polynomial time, i.e., the computational time is polynomial in the length of the prediction horizon [31]. In the application, the prediction horizon is relatively short because it is limited by the accuracy of the short-term prediction, which worsens with a growing horizon.

V. Numerical Study

In this section, the performance of the proposed EMS is analyzed and compared with an SoC reference tracking MPC based on the simulation of a real-world driving cycle. The study considers a passenger vehicle equipped with a FCS with a nominal power of $55\,\mathrm{kW}$ and a battery with a capacity of $9.9\,\mathrm{kWh}$. The steady-state measurement data of the FCS's fuel consumption rate and the approximation with the polynomial model according to (23) are shown in Fig. 5. The actual fuel consumption for the driving mission is computed by interpolating in the map of measurements, whereas the offline optimization and the online MPC operate with the polynomial model. The battery parameters were identified based on measurement data resulting in $V_{\mathrm{OC}} = 350\,\mathrm{V}$, $R_{\mathrm{int}} = 0.15\,\Omega$, and $Q_0 = 28.28\,\mathrm{Ah}$. The vehicle mass is $1950\,\mathrm{kg}$.

The control-relevant system constraints are $5\,\mathrm{kW} \leq P_{\mathrm{FCS}} \leq 55\,\mathrm{kW}$, $-30\,\mathrm{kW} \leq P_{\mathrm{b}} \leq 50\,\mathrm{kW}$, $0.3 \leq \xi \leq 0.9$, and the FCS power rate is constrained with $\pm 25\,\mathrm{kW/s}$. The initial SoC is 0.7 and the final SoC ≥ 0.7. The MPCs operate with a sampling time of $1\,\mathrm{s}$ and a prediction horizon of $30\,\mathrm{s}$.

The remainder of this section is structured as follows: First, the SoC reference tracking MPC is introduced in Section V-A, followed by the description of the driving cycle and the predictions in Section V-B. The optimization based on the long-term prediction and the corresponding results are discussed in Section V-C. Finally, the performances of the MPCs are compared and evaluated in Section V-D, and the effect of the prediction horizon length is discussed in Section V-E.

A. SoC Reference Tracking MPC

The proposed cost-to-go MPC is compared with an MPC that tracks an SoC reference trajectory at the end of the prediction horizon. The linear formulation of the SoC reference tracking MPC is analogous to the formulation of the cost-to-go MPC presented in Section IV, but instead of considering the cost-to-go, the deviation from the SoC reference is penalized at the end of the prediction horizon:

$$p_{\xi,k+N_\mathrm{p}} = q_{\mathrm{track}} \left(\xi^{\mathrm{ref}}_{k+N_\mathrm{p}} - \xi_{k+N_\mathrm{p}} \right)^2. \tag{34}$$

Thus, the overall objective function to be minimized according to (11) is

$$J^{\mathrm{track}}_k = m_{\mathrm{H_2},k} + m_{\mathrm{eq},k} + p_{\xi,k+N_\mathrm{p}}. \tag{35}$$

The tracking weighting q_{track} is $10^6\,\mathrm{g}$ in this study, which ensures that the SoC reference at the end of the prediction horizon is tracked sufficiently close. The remaining parameters are chosen identically as for the cost-to-go MPC.

The SoC reference is the optimal trajectory according to the long-term prediction of the driving mission. The optimization is conducted by the DP algorithm (9), whereby the optimal control inputs $P^*_{\mathrm{FCS},l}(\xi_l)$ are stored for each position of the distance grid. After the optimization, the optimal SoC trajectory can be computed in forward direction starting at ξ_0 and linearly interpolating in the map of optimal control inputs.

B. Driving Cycle and Predictions

The velocity and altitude data of the driving cycle were recorded on a real-world drive covering $210\,\mathrm{km}$, and the electric power demand was derived based on the vehicle model (1) – (3) assuming a constant auxiliary power of $2\,\mathrm{kW}$ (see upper two plots of Fig. 6). The driving cycle starts and ends in urban areas and includes rural road and highway sections. The first half of the cycle goes uphill overcoming an altitude gain of approximately $730\,\mathrm{m}$. Therefore, the highway section between kilometers 30 and 100 shows a comparably high power demand.

In this study, the long-term prediction of the velocity (see Fig. 6) was retrieved from legal speed limits using *AVL Route Studio*, which is a test cycle preparation tool. The tool considers vehicle dynamics during acceleration phases and limits the cornering speed depending on the road curvature. The comparison with the actual velocity profile shows that the long-term prediction provides a good estimate of the actual velocity for a significant fraction of the driving cycle. In some sections, however, the long-term prediction deviates considerably from the actual velocity. The most obvious deviation is between kilometers 126 and 141 and was caused by roadworks on the highway.

The focus of this study is to analyze the potential of the proposed EMS and to what extent an accurate online velocity prediction can be beneficial for the energy management. For this purpose, the short-term prediction is assumed to be ideal, i.e., coinciding with the actual velocity.

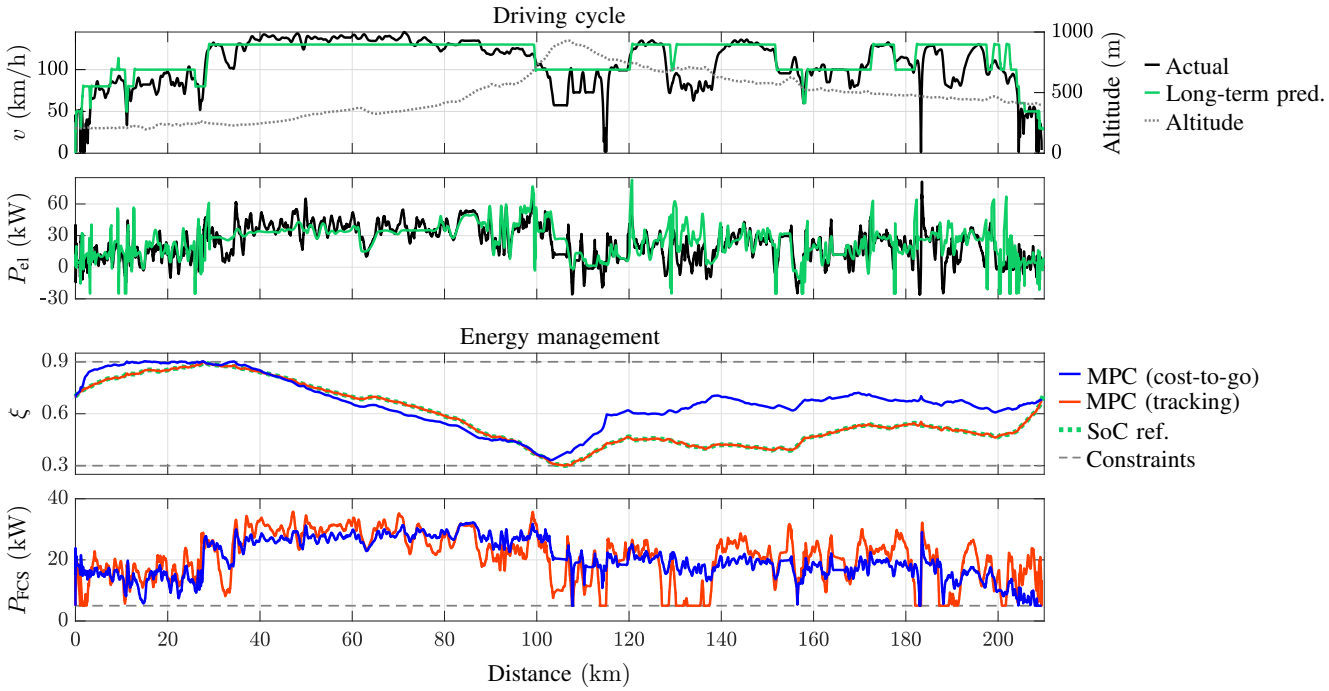

Fig. 6: Upper plots: Actual data and long-term predictions for the investigated real-world driving cycle. Lower plots: SoC and FCS power resulting under the control of the two MPCs.

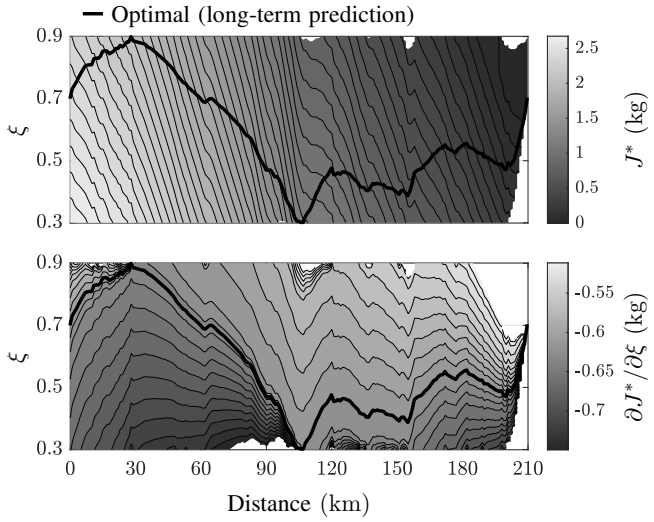

Fig. 7: Optimal cost-to-go (upper plot) and partial derivative of the optimal cost-to-go with respect to the SoC (lower plot) as a function of the position and the SoC. Both plots include the optimal SoC trajectory according to the long-term prediction. Note that extreme values are excluded in the lower plot for a better visualization.

C. Offline Optimization

For the offline optimization, the feasible ranges of the SoC and the FCS power are quantized with 120 and 40 grid segments, respectively, and the step size of the distance grid is chosen to be 1 km. The resulting 2-D optimal cost-to-go map depending on the position and the SoC is depicted in the upper plot of Fig. 7. It can be seen that the cost-to-go decreases with the covered distance and with an increasing SoC. White areas indicate infeasible ranges according to the long-term prediction and the specified constraints. The plot includes the globally optimal SoC trajectory according to the long-term prediction, which is used as reference trajectory in the SoC reference tracking MPC. The optimal SoC trajectory uses the whole feasible SoC range, which indicates the importance of considering state constraints in the DP.

The lower plot of Fig. 7 depicts the partial derivative of the cost-to-go with respect to the SoC. It can be shown that the derivative of the cost-to-go corresponds to the SoC-related costate in Pontryagin's minimum principle (PMP) [23]. The Hamiltonian of PMP is independent of the SoC with the chosen battery model. Consequently, the costate is constant along optimal paths within sections where no constraints are active [32]. This means that the level lines in the lower plot of Fig. 7 illustrate optimal paths for reaching the destination from any position and feasible SoC. A subset of the optimal paths meet at points where the SoC constraints are active, i.e., at the kilometers 28 and 106, causing a discontinuous change of the costate. The behavior due to active SoC constraints also causes the sharp changes in the slope of the $\partial J^*/\partial\xi$ profile (see lower plots of Fig. 4).

D. Performance Evaluation

The SoC and FCS power trajectories resulting under the control of the two MPCs are depicted in the lower two plots of Fig. 6. Besides analyzing their behavior, the two MPCs are compared quantitatively based on two performance measures: the specific fuel consumption and an equivalent number of

TABLE I: Comparison of specific fuel consumption and equivalent number of FCS load cycles regarding the investigated driving cycle

EMS	m_{fuel}	Rel. diff.	N_{eq}	Rel. diff.
Optimal	11.25 g/km	−0.3 %	14.2	+15 %
Cost-to-go MPC	11.28 g/km	0.0 %	12.4	0 %
SoC ref. track. MPC	11.32 g/km	+0.4 %	17.1	+38 %

FCS load cycles [33], which is defined by

$$N_{\text{eq}} = \frac{1}{2P_{\text{FCS}}^{\max}} \int_{t_0}^{t_1} \left| \frac{\mathrm{d}P_{\text{FCS}}}{\mathrm{d}t} \right| \mathrm{d}t \tag{36}$$

and can be interpreted as a measure for degradation [34].

The SoC reference tracking MPC tracks the SoC reference at the end of the prediction horizon but can deviate from the reference within the horizon to adapt the power split according to the short-term prediction. However, the 30 s prediction horizon does not provide much freedom, and the MPC tracks the SoC reference, which is based on the long-term prediction, rather strictly. Consequently, the FCS power signal shows fluctuations depending on the deviation of the predicted power demand from the actual power demand. The fluctuating behavior stresses the FCS and affects the fuel efficiency.

Unlike the SoC tracking MPC, the proposed cost-to-go MPC is provided with optimized long-term information available for the entire SoC range and does not rely on a single reference trajectory. Thus, the MPC has more freedom to compensate for deviations of the long-term power demand prediction. The resulting FCS power trajectory is smoother, which improves the fuel performance and mitigates FCS degradation.

Tab. I compares the specific fuel consumption and the equivalent number of load cycles of the two MPCs and the overall optimal energy management minimizing the fuel consumption. For the investigated driving cycle, the cost-to-go MPC achieves a 0.4 % lower fuel consumption than the SoC tracking MPC, even though the predictions are identical for both MPCs. This improvement is remarkable considering that the theoretical optimum is only 0.3 % better than the result of the cost-to-go MPC. The performance advantage of the cost-to-go MPC over the SoC tracking MPC is even more impressive regarding the equivalent number of FCS load cycles, where an improvement of 38 % is achieved. To sum up, the cost-to-go MPC does not only improve the fuel efficiency but also stresses the FCS considerably less, which potentially mitigates degradation. Both methods satisfy all specified constraints.

The operation of the two MPCs is compared in more detail during the roadworks section between kilometers 126 and 141, where the power demand prediction based on static route data deviates considerably from the actual power demand. The comparison is shown in Fig. 8, whereby the SoC at the beginning of the section is set identical in both cases for a better illustration. The long-term prediction estimated a high power demand for the section. Therefore, the optimized SoC reference decreases meaning that the battery is expected

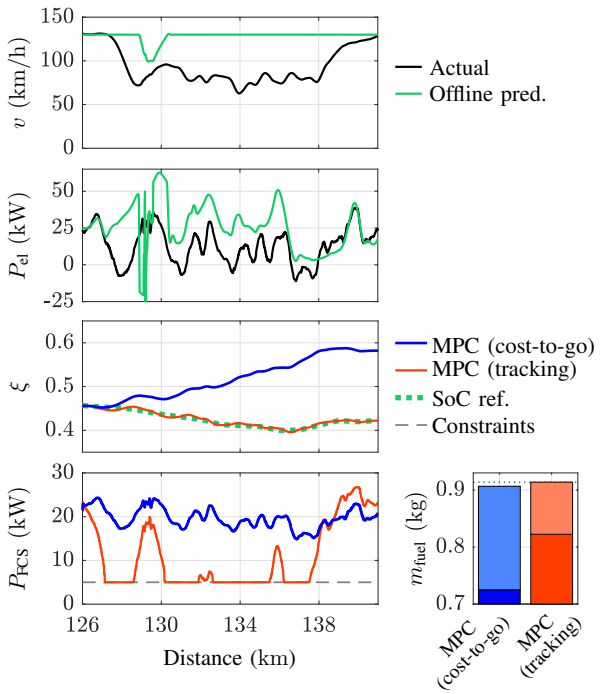

Fig. 8: Study of the two MPCs during the roadworks section, where the initial SoC is set identical in both cases. The bar chart compares the corresponding optimal costs-to-go at the end of the section (lower, dark parts), costs within the section (upper, light parts), and total costs.

to support the FCS. However, the actual power demand is significantly lower. The SoC tracking MPC drastically reduces the FCS power to follow the reference trajectory hitting the lower boundary on the FCS power. On the contrary, the cost-to-go MPC maintains the FCS power at a high level and even charges the battery. As the SoC rises, the cost-to-go MPC only gradually lowers the FCS power according to the optimum with the cost-to-go. Operating the FCS with a higher power implies a higher amount of fuel consumed *within* the section compared to the SoC tracking MPC (see upper parts of bar chart in Fig. 8). However, the cost-to-go MPC achieves a lower cost-to-go at the end of the section, which overcompensates for the higher cost within the section. Consequently, the total cost m_{fuel}, i.e., the sum of the fuel consumed within the section and the cost-to-go at the end of the section, is 7 g lower than for the SoC tracking MPC. Note that this improvement only refers to the investigated section with a length of 15 km.

E. Effect of the Prediction Horizon Length

Fig. 9 shows the comparison of the two MPCs regarding the fuel consumption and the equivalent number of FCS load cycles as a function of the prediction horizon length. The cost-to-go MPC significantly outperforms the SoC tracking MPC regarding both measures, in particular if the prediction horizon is short. For an 1-step prediction horizon, the tracking MPC leads to a 2.3 % higher fuel consumption and the equivalent number of load cycles is even 12-fold. The tracking MPC approaches the performance of the cost-to-go MPC with

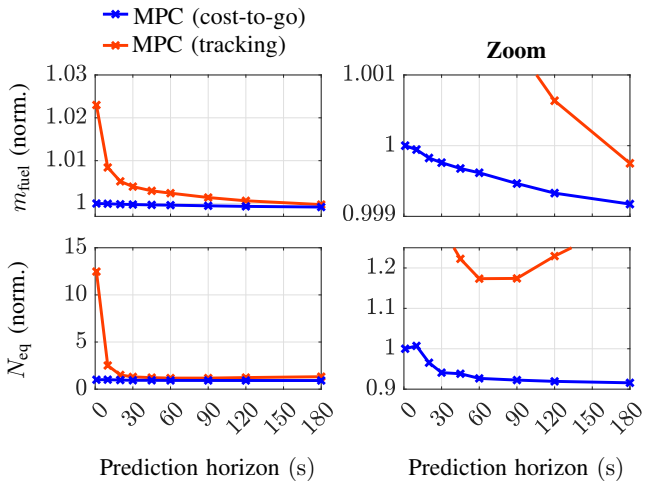

Fig. 9: Comparison of the fuel consumption and the equivalent number of FCS load cycles (both normalized) as a function of the prediction horizon.

an increasing prediction horizon and achieves a comparable performance only for rather long prediction horizons, where short-term predictions are expected to be less accurate.

The fuel performance under the cost-to-go MPC is already decent with an 1-step prediction horizon and improves further with growing prediction horizon. Also, the equivalent number of load cycles decreases; a 30 s prediction horizon reduces the number of load cycles by approximately 6 %.

The investigation suggests that the cost-to-go MPC also performs well if the prediction horizon varies throughout the driving mission, e.g., a short horizon in urban areas and a longer horizon on the highway.

VI. Conclusion

A predictive EMS was proposed that efficiently combines a long-term prediction derived from *a-priori* available static route information and real-time short-term predictions from vehicular communication systems. Before departure, a DP algorithm optimizes the power split between the FCS and the battery based on the long-term prediction yielding the optimal cost-to-go as a function of the position and the SoC. The online energy management is determined by an MPC that minimizes the fuel consumption considering the short-term predictions within the prediction horizon and the optimal cost-to-go as terminal cost. A linear formulation of the MPC with a physically motivated objective function was developed, which is highly beneficial for the real-time, onboard execution of the EMS.

The proposed EMS was compared with an SoC reference tracking MPC in simulation. Tracking the optimized SoC reference trajectory showed to be too restrictive to actually benefit from the short-term predictions. On the contrary, the cost-to-go MPC optimized the power split independently from the SoC based on the optimum according to the combined long-term and short-term information. The cost-to-go MPC clearly outperformed the SoC reference tracking MPC regarding the fuel efficiency and the equivalent number of load cycles, which can be interpreted as degradation measure, in particular if the short-term prediction horizon is short.

References

[1] S. C. de Almeida and R. Kruczan, "Effects of drivetrain hybridization on fuel economy, performance and costs of a fuel cell hybrid electric vehicle," *International Journal of Hydrogen Energy*, vol. 46, no. 79, pp. 39 404–39 414, 2021. [Online]. Available: https://doi.org/10.1016/j.ijhydene.2021.09.144

[2] P. Thounthong, V. Chunkag, P. Sethakul, B. Davat, and M. Hinaje, "Comparative study of fuel-cell vehicle hybridization with battery or supercapacitor storage device," *IEEE Transactions on Vehicular Technology*, vol. 58, no. 8, pp. 3892–3904, 2009. [Online]. Available: https://doi.org/10.1109/TVT.2009.2028571

[3] G. G. Nassif and S. C. de Almeida, "Impact of powertrain hybridization on the performance and costs of a fuel cell electric vehicle," *International Journal of Hydrogen Energy*, vol. 45, no. 41, pp. 21 722–21 737, 2020. [Online]. Available: https://doi.org/10.1016/j.ijhydene.2020.05.138

[4] M. Koot, J. Kessels, B. de Jager, W. Heemels, P. van den Bosch, and M. Steinbuch, "Energy management strategies for vehicular electric power systems," *IEEE Transactions on Vehicular Technology*, vol. 54, no. 3, pp. 771–782, 2005. [Online]. Available: https://doi.org/10.1109/TVT.2005.847211

[5] J. Ziegmann, J. Shi, T. Schnörer, and C. Endisch, "Analysis of individual driver velocity prediction using data-driven driver models with environmental features," in *2017 IEEE Intelligent Vehicles Symposium (IV)*, 2017, pp. 517–522. [Online]. Available: https://doi.org/10.1109/IVS.2017.7995770

[6] J. Shin and M. Sunwoo, "Vehicle speed prediction using a markov chain with speed constraints," *IEEE Transactions on Intelligent Transportation Systems*, vol. 20, no. 9, pp. 3201–3211, 2019. [Online]. Available: https://doi.org/10.1109/TITS.2018.2877785

[7] Z. Zhou, Z. Yang, Y. Zhang, Y. Huang, H. Chen, and Z. Yu, "A comprehensive study of speed prediction in transportation system: From vehicle to traffic," *iScience*, vol. 25, no. 3, p. 103909, 2022. [Online]. Available: https://doi.org/10.1016/j.isci.2022.103909

[8] S. Zendegan, A. Ferrara, S. Jakubek, and C. Hametner, "Predictive battery state of charge reference generation using basic route information for optimal energy management of heavy-duty fuel cell vehicles," *IEEE Transactions on Vehicular Technology*, vol. 70, no. 12, pp. 12 517–12 528, 2021. [Online]. Available: https://doi.org/10.1109/TVT.2021.3121129

[9] D. Shen, L. Lu, and S. Müller, "Utilization of predictive information to optimize driving and powertrain control of series hybrid vehicles," *Automotive and Engine Technology*, vol. 2, no. 1, pp. 39–47, 2017. [Online]. Available: https://doi.org/10.1007/s41104-017-0016-6

[10] S. Kelouwani, N. Henao, K. Agbossou, Y. Dube, and L. Boulon, "Two-layer energy-management architecture for a fuel cell hev using road trip information," *IEEE Transactions on Vehicular Technology*, vol. 61, no. 9, pp. 3851–3864, 2012. [Online]. Available: https://doi.org/10.1109/TVT.2012.2214411

[11] J. Pei, Y. Su, D. Zhang, Y. Qi, and Z. Leng, "Velocity forecasts using a combined deep learning model in hybrid electric vehicles with V2V and V2I communication," *Science China Technological Sciences*, vol. 63, no. 1, pp. 55–64, 2020. [Online]. Available: https://doi.org/10.1007/s11431-018-9396-0

[12] W. Zhou, L. Yang, T. Ying, J. Yuan, and Y. Yang, "Velocity prediction of intelligent and connected vehicles for a traffic light distance on the urban road," *IEEE Transactions on Intelligent Transportation Systems*, vol. 20, no. 11, pp. 4119–4133, 2019. [Online]. Available: https://doi.org/10.1109/TITS.2018.2882609

[13] Y. Li, H. He, and J. Peng, "An adaptive online prediction method with variable prediction horizon for future driving cycle of the vehicle," *IEEE Access*, vol. 6, pp. 33 062–33 075, 2018. [Online]. Available: https://doi.org/10.1109/ACCESS.2018.2840536

[14] C. Sun, S. J. Moura, X. Hu, J. K. Hedrick, and F. Sun, "Dynamic traffic feedback data enabled energy management in plug-in hybrid electric vehicles," *IEEE Transactions on Control Systems Technology*, vol. 23, no. 3, pp. 1075–1086, 2015. [Online]. Available: https://doi.org/10.1109/TCST.2014.2361294

[15] Q. Gong, Y. Li, and Z.-R. Peng, "Trip based power management of plug-in hybrid electric vehicle with two-scale dynamic programming," in *2007 IEEE Vehicle Power and Propulsion Conference*, 2007, pp. 12–19. [Online]. Available: https://doi.org/10.1109/VPPC.2007.4544089

[16] X. Zhang, L. Guo, N. Guo, Y. Zou, and G. Du, "Bi-level energy management of plug-in hybrid electric vehicles for fuel economy and battery lifetime with intelligent state-of-charge reference," *Journal of Power Sources*, vol. 481, p. 228798, 2021. [Online]. Available: https://doi.org/10.1016/j.jpowsour.2020.228798

[17] L. Fu, Ü. Özgüner, P. Tulpule, and V. Marano, "Real-time energy management and sensitivity study for hybrid electric vehicles," in *Proceedings of the 2011 American Control Conference*, 2011, pp. 2113–2118. [Online]. Available: https://doi.org/10.1109/ACC.2011.5991374

[18] V. Larsson, L. J. Mårdh, and B. Egardt, "Comparing two approaches to precompute discharge strategies for plug-in hybrid electric vehicles," *IFAC Proceedings Volumes*, vol. 46, no. 21, pp. 121–126, 2013, 7th IFAC Symposium on Advances in Automotive Control. [Online]. Available: https://doi.org/10.3182/20130904-4-JP-2042.00114

[19] V. Larsson, "Route optimized energy management of plug-in hybrid electric vehicles," Ph.D. dissertation, 2014. [Online]. Available: https://publications.lib.chalmers.se/records/fulltext/196399/196399.pdf

[20] L. Johannesson and B. Egardt, "A novel algorithm for predictive control of parallel hybrid powertrains based on dynamic programming," *IFAC Proceedings Volumes*, vol. 40, no. 10, pp. 343–350, 2007, 5th IFAC Symposium on Advances in Automotive Control. [Online]. Available: https://doi.org/10.3182/20070820-3-US-2918.00047

[21] C. Zhang and A. Vahidi, "Route preview in energy management of plug-in hybrid vehicles," *IEEE Transactions on Control Systems Technology*, vol. 20, no. 2, pp. 546–553, 2012. [Online]. Available: https://doi.org/10.1109/TCST.2011.2115242

[22] S. M. Sotoudeh and B. HomChaudhuri, "Robust Predictive Energy Management of Connected Power-Split Hybrid Electric Vehicles Using Dynamic Traffic Data," *Journal of Dynamic Systems, Measurement, and Control*, vol. 144, no. 1, 01 2022, 014501. [Online]. Available: https://doi.org/10.1115/1.4053291

[23] H. Borhan, A. Vahidi, A. M. Phillips, M. L. Kuang, I. V. Kolmanovsky, and S. Di Cairano, "MPC-based energy management of a power-split hybrid electric vehicle," *IEEE Transactions on Control Systems Technology*, vol. 20, no. 3, pp. 593–603, 2012. [Online]. Available: https://doi.org/10.1109/TCST.2011.2134852

[24] D. Mayne, "Nonlinear model predictive control:challenges and opportunities," in *Nonlinear Model Predictive Control*, F. Allgöwer and A. Zheng, Eds. Basel: Birkhäuser Basel, 2000, pp. 23–44. [Online]. Available: https://doi.org/10.1007/978-3-0348-8407-5_2

[25] L. Guzzella and A. Sciarretta, *Vehicle Propulsion Systems: Introduction to Modeling and Optimization*. Berlin, Heidelberg: Springer Berlin Heidelberg, 2013. [Online]. Available: https://doi.org/10.1007/978-3-642-35913-2_2

[26] D. E. Kirk, *Optimal Control Theory: An Introduction*. Dover Publications, 2004.

[27] S. Kofler, Z. P. Du, S. Jakubek, and C. Hametner, "Adaptive step size dynamic programming for optimal energy management of fuel cell vehicles," in *2023 IEEE Vehicle Power and Propulsion Conference (VPPC)*, in press.

[28] F. Borrelli, A. Bemporad, and M. Morari, *Predictive Control for Linear and Hybrid Systems*. Cambridge University Press, 2017. [Online]. Available: https://doi.org/10.1017/9781139061759

[29] L. Wang, *Model Predictive Control System Design and Implementation Using MATLAB®*, 1st ed. Springer London, 2009. [Online]. Available: https://doi.org/10.1007/978-1-84882-331-0

[30] S. Onori and L. Tribioli, "Adaptive Pontryagin's minimum principle supervisory controller design for the plug-in hybrid GM Chevrolet Volt," *Applied Energy*, vol. 147, pp. 224–234, 2015. [Online]. Available: https://www.sciencedirect.com/science/article/pii/S0306261915000276

[31] S. A. Vavasis, *Complexity Theory: Quadratic Programming*. Boston, MA: Springer US, 2001, pp. 304–307. [Online]. Available: https://doi.org/10.1007/0-306-48332-7_65

[32] H. P. Geering, *Optimal Control with Engineering Applications*. Berlin, Heidelberg: Springer Berlin Heidelberg, 2007. [Online]. Available: https://doi.org/10.1007/978-3-540-69438-0

[33] A. Ferrara, S. Jakubek, and C. Hametner, "Energy management of heavy-duty fuel cell vehicles in real-world driving scenarios: Robust design of strategies to maximize the hydrogen economy and system lifetime," *Energy Conversion and Management*, vol. 232, p. 113795, 2021. [Online]. Available: https://doi.org/10.1016/j.enconman.2020.113795

[34] P. Pei, Q. Chang, and T. Tang, "A quick evaluating method for automotive fuel cell lifetime," *International Journal of Hydrogen Energy*, vol. 33, no. 14, pp. 3829–3836, 2008, tMS07: Symposium on Materials in Clean Power Systems. [Online]. Available: https://doi.org/10.1016/j.ijhydene.2008.04.048